Title:

Performance of sheet pile as a seismic retrofit for old piled abutment subjected to liquefaction-induced lateral spreading

Authors:

Partha Saha

Housing and Building Research Institute, Bangladesh (Formerly, Tokyo Institute of Technology, Japan)

Kazuki Horikoshi

Assistant Professor, Department of Civil and Environmental Engineering, Tokyo Institute of Technology, Japan

Akihiro Takahashi

Professor, Department of Civil and Environmental Engineering, Tokyo Institute of Technology, Japan

Soil Dynamics and Earthquake Engineering, 141, 106507, 2021

Official URL:

https://doi.org/10.1016/j.soildyn.2020.106507

Abstract

Liquefaction-induced lateral spreading causes severe damage to the pile foundation of structures. Old structures that are not properly designed for liquefaction are more vulnerable to a strong earthquake. Many old piled abutments require a remedial measure against lateral spreading. This paper examines the responses of an old piled abutment subjected to liquefaction-induced lateral spreading and efficacy of the sheet pile reinforcement technique to mitigate the associated damage through dynamic centrifuge experiments. The experiment on the old piled abutment reveals that the abutment moves together with the spreading soil and shows a significant channel-ward movement without pinning effect. The large bending moments are found to take place around the pile head and the interface of the loose and the dense layer as expected. The installation of sheet pile in front of the abutment considerably reduces the channel-ward movement of the abutment thus mitigate the bending moment demand of the piles.

Keywords

Seismic retrofit; Centrifuge experiment; Piled abutment; Lateral spreading; Liquefaction; Sheet pile

1. Introduction

The liquefaction-induced lateral spreading can cause great damage to the pile foundations. Numerous observations of pile failure have been documented in the previous major earthquakes [1][2][3]. The waterfront structures, for example, the bridge foundations resting on a liquefiable layer, are particularly vulnerable due to the lateral spreading [4][5]. A large number of bridge foundations are observed to fail or to be severely damaged due to the liquefaction or the liquefaction-induced lateral spreading of the loose foundation in the past earthquakes [1][6][7][8][9][10]. Because of the lateral spreading of the liquefied soils, the waterfront structures go under significant water-ward displacement. The lateral spreading is highly damaging if the loose sand layer is overlain by a non-liquefiable crust [11][12]. The non-liquefiable crustal layer can push the structure more since it does not lose its strength due to the liquefaction of the underlying sand. The bridge abutment, which is the first support of a river-spanning bridge, carries the load from the superstructure as well as it retains the approach embankment which is usually non-liquefiable. Thus, the piled abutment is probably the most crucial structural element of a river crossing bridge that can be severely damaged due to the lateral spreading of the loose foundation that needs more attention.

Extensive researches have been conducted to observe the response of the pile foundation subjected to lateral spreading. Large-scale shake table tests are conducted to observe the response of a pile group in a liquefied soil on the level ground and as well as on the sloping ground [13][14][15][16]. Wang et al. [17] conducted several shake-table tests to investigate the scouring effect of the crusts on the seismic behaviour of the pile-supported bridge piers resting in liquefiable soil. The scouring of the crusts was observed to make the inertial effect more dominant than the Kinematic effect. Motamed et al. [18] carried out a large scale shake

table test (E-Defense) to determine the response of the pile group behind a quay wall subjected to lateral spreading. The pile tips in those experiments described in the above-mentioned articles were kept either fixed or pinned to the bottom of the container. However, the actual response of the pile group is neither perfectly fixed nor pinned, which might affect the response of the pile group. Brandenberg et al. [19] conducted several centrifuge experiments to study the behaviour of pile foundation in laterally spreading ground to characterize the soil-pile interaction in the liquefied ground. They conclude that the response of the pile in the liquefied ground is significantly influenced by its relative stiffness.

Although a large number of research works exist on the response of the pile foundation in the laterally spreading ground, however, the behaviour of the piled abutment is rarely studied. The centrifuge model tests and finite element analysis by Takahashi et al. [20][21] are a few of the limited number of studies. Saha and Takahashi [22] and Saha et al. [23][24] also studied the behaviour of the piled abutment by the finite element analysis. These studies were motivated by the fact that the piled abutments designed according to the old Japanese design guideline for highway bridges[25] are not resilient enough to sustain in a very strong earthquake as the liquefaction effects are not considered in the design.

The liquefaction-induced damage to the pile foundation can be remediated either by improving the ground against liquefaction or mitigating the lateral spreading through reinforcement. The ground improvement techniques to mitigate liquefaction, such as ground densification, were found effective in the experiments as well as in the previous earthquakes [26][27][28][29][30][31][32]. However, ground improvement techniques are difficult to implement for the existing structures. Pamuk et al. [33] implemented a passive site stabilization technique by using colloidal silica to remediate the piled foundation against

lateral spreading. Although this passive stabilization technique looks attractive for the existing structures, the seepage flow might hinder the efficiency of this technique near a water body. Considering all the limitations to implement the ground improvement techniques, the authors consider using the sheet pile reinforcement technique to mitigate the lateral spreading of a loose foundation, thus preventing the failure of the pile foundations. Motamed and Towhata [34] implemented a sheet pile to improve the performance of a pile group behind the quay wall subjected to lateral spreading. The fixed end sheet pile was found effective to mitigate the effect of lateral spreading, for instance, on reduction in the bending moment of the piles behind the sheet pile. Further study is needed to ensure the efficiency of the sheet pile to mitigate lateral spreading since it is affected by the softening of the bearing stratum caused by the generation of excess pore water pressure.

In this study, to examine the efficiency of the sheet pile as a seismic retrofit for an old piled abutment subjected to liquefaction-induced lateral spreading, four dynamic centrifuge experiments are carried out. The experiments are conducted under different reinforcement and structural configurations. One experiment is conducted without any sheet pile reinforcement to study the seismic response of the old piled abutment subjected to lateral spreading. Whereas, the bridge abutment is reinforced with sheet pile in the other experiment to determine the efficiency of the sheet pile as a seismic retrofit. Other two experiments are conducted without any bridge abutment having the same geometric configurations to examine the ground movement in the reinforced and unreinforced condition. The results are compared with the cases with an abutment to investigate the pinning effect of the pile foundation. Pile pinning effect is the reduction of the lateral spreading caused by the pile foundation. It should be mentioned that the bridge girder is not modelled in this study and the strut effect of bridge girder is not considered here for simplicity.

2. Experimental program

2.1. Test conditions

Four dynamic centrifuge experiments are carried out at 50 g using the Tokyo tech Mark III centrifuge facility [35]. The experiments are conducted to study the seismic response of the old bridge abutment resting in a liquefiable layer and simultaneously investigate the efficacy of the sheet pile as a seismic retrofit for the piled abutment. The test conditions are summarised in Table 1. A generalized scaling law [36] is used to model the ground and the structural elements in these experiments. The generalized scaling law allows using the combined scaling law of a 1 g shake table experiment and a 50 g centrifuge experiment to accommodate a large prototype within a limited dimension in the centrifuge. The combined scaling factor for a 1:2 scaled shake table experiment and 50 g centrifuge experiment is used here. The scaling factor for different important parameters, for example, length, acceleration, bending stiffness, etc. are tabulated in Table 2. Two centrifuge experiments (C-5 and C-6) consist of a piled abutment. The piles of the abutment pass through an 8 m thick loose layer while the pile tips are embedded 14 m into the dense ground. Whereas, the experimental cases C-1 and C-3 are conducted without any abutment to investigate the pinning effect of pile foundation. The experimental results of C-1 and C-3 have been already reported in another paper [37]. The model ground is reinforced with sheet pile to mitigate lateral spreading of the loose foundation in C-3 and C-6. The typical model ground consists of an 8 m thick approach embankment (having a side slope 1:2) of a river spanning bridge resting on a layered foundation. The top 8 m of the foundation ground is made of loose liquefiable sand (Dr = 50%) that is resting on a 15 m thick dense layer (Dr = 90%). The water table is set at the foundation ground surface. The detailed plan and cross-sectional views of the experimental

133 cases are shown in Figs. 1 and 2. The approach embankment is also made of loose sand (Dr =
134 50%) to avoid unexpected densification of the liquefiable foundation. The model ground
135 consisting of the approach embankment as well as the foundation ground is made of Toyoura
136 sand in the centrifuge experiment. The physical properties of the Toyoura sand are tabulated
137 in Table 3.

138 The model abutment is placed at the channel end of the approach embankment, as shown in
139 Fig. 2. The half-width of a 3×8 piled abutment is modelled to get the advantage of symmetry.
140 Therefore, the abutment is placed at the side of the container in the centrifuge experiment.
141 The abutment and the piles are designed according to the old Japanese design standard of
142 highway bridges [25]. The wing wall, vertical wall, and the footing of the abutment in the
143 centrifuge experiment are made of aluminium. The specifications of the model abutment are
144 tabulated in Table 4. The abutments are usually made of reinforced concrete in reality.
145 Therefore, the generalized scaling factor for density (which is 1.0) of the abutment is not
146 satisfied with the abutment. However, the total mass and centre of the gravity of the
147 abutment are estimated and modelled according to the appropriate scaling factor. Therefore,
148 the authors believe that the deviation of the generalized scaling factor for the density of the
149 abutment doesn't significantly affect the overall response of the structural system.

150 The half abutment is supported by 12 piles according to the actual design. However, it is
151 difficult to model 12 piles with instrumentation in the limited space of the centrifuge
152 experiment. Therefore, a simplification is applied in the design of the model abutment. The
153 frame formed with the piles rigidly connected to the abutment footing at their heads can be
154 treated as a shear frame by considering the footing is infinitely rigid in comparison with the
155 piles. Therefore, the three-column shear frame along the longitudinal axis can be modelled as

156 an equivalent two-column shear frame by increasing the bending stiffness of each pile 1.5
157 times as that of the pile in the prototype [38]. Similarly, in the transverse direction, the piles
158 in four rows are converted into two rows by increasing the bending stiffness two times as that
159 of the original pile. Therefore, each pile in the simplified model corresponds to the three piles
160 in the prototype. The concept of this simplification is illustrated in Fig. 3. In the experiment,
161 four rectangular acrylic piles are used to support the abutment in the centrifuge experiment.
162 The details of the model abutment are shown in Fig. 4.

163 The abutment piles are usually failed due to bending in the incidence of lateral spreading.
164 Therefore, the bending stiffness of the pile should be properly modelled in the centrifuge
165 experiment. However, the circular RC pile in the prototype cannot be directly modelled in the
166 centrifuge experiment. Therefore, the acrylic pile with appropriate bending stiffness is used.
167 Besides, the rectangular shape provides a wide surface for the instrumentation of the strain
168 gauges as well as the slender behaviour of the abutment piles can be simulated in the
169 experiment. The rectangular piles in the experiment might attract comparatively larger
170 kinematic load than the circular piles which is one of the limitations of the centrifuge
171 modelling. Since the slender piles move with the liquefied ground during lateral spreading the
172 authors believe that the rectangular shape doesn't affect much in the overall response of the
173 structural system.

174 The head of the piles is rigidly attached to the abutment footing. Whereas, the tip of the piles
175 is kept free inside the ground. Two piles out of four are instrumented with strain gauges to
176 measure the bending moment at different depths. The instrumented piles (Pile type-A) are
177 attached to the abutment at the opposite side of the container wall as shown in Fig. 2. The
178 dimensions of the pile and the locations of the strain gauges on the pile are shown in Fig. 5.

The specifications of the acrylic piles together with those aimed in the prototype are listed in Table 5.

It is already mentioned that the sheet pile reinforcement is used in this study. A 2.5 mm thick steel plate (in model scale) is used as sheet pile here. The sheet pile is embedded 14 m deep into the dense layer to mitigate the lateral spreading of the overlying loose sand. The top of the sheet pile is extended 3 m into the non-liquefiable embankment. The top and the tip of the sheet pile are kept free. A full-width sheet pile is used in C-3, as shown in Fig. 1 (b). In the case of full-width sheet pile, three separate plates are used (see Fig. 1 (b)). The primary purpose of using sheet pile is to mitigate the effect of lateral spreading in the region located 50 mm (in model scale that corresponds to 5 m in prototype) in the transverse direction from the container wall. The other two plates are placed to avoid the effect of ground movement beside the desired protected zone. However, it was found that the extension of the sheet pile width beyond the target area did not have any additional advantage to mitigate the lateral spreading of the target area [37]. Therefore, the region only in front of the abutment is reinforced with sheet pile in C-6. The 5 m width (in prototype) sheet pile is instrumented with strain gauges to measure the bending moment at different depths. The instrumentation of the sheet pile is shown in Fig. 6. The specifications of the sheet pile are tabulated in Table 6.

2.2. Model preparation

The ground is prepared in a rigid container having the inner dimensions of 600 mm, 250 mm, and 400 mm in length, width, and height, respectively. Toyoura sand is used to prepare the model ground in all the experiments. An air pluviation method is used to pour the sand into the container by using a sand-hopper. The different relative densities in the different layers

202 are maintained by changing the pouring rate and the falling height of the sand, which is
203 calibrated before the ground preparation. The actual relative densities of different layers in
204 all the cases are tabulated Table 1. The foundation ground (15 m thick dense sand overlain by
205 an 8 m thick loose sand) is saturated with the de-aerated Metolose (60-SH50) solution (2.2%
206 by weight) to make the viscosity of the pore fluid 50 times as that of the water [39]. Metolose
207 is the commercial name of Hydroxypropyl Methylcellulose from Shin-Etsu Chemical Company.
208 According to the generalized scaling law, the viscosity should be 70.71 times of water.
209 However, due to the difficulties in saturating the model ground with high viscous fluid, the
210 viscosity of the pore fluid is kept 50 times the viscosity of water. Thus, the permeability of the
211 soils is relatively larger and this might cause a relatively faster dissipation of the excess pore
212 water pressure. The piles of the abutment, as well as the sheet pile, are usually driven into the
213 ground in practice. However, the sheet pile and the abutment piles are placed into the
214 container before the soil is poured due to the ease of model preparation. Therefore, the effect
215 of the ground densification due to the driven piles and sheet piles, in reality, cannot be
216 simulated in the experiment.

217 The ground response characterised by the surface settlement, horizontal ground movement,
218 generation of excess pore water pressure and the seismic acceleration at different depth is
219 properly recorded during the experiment. A sufficient number of sensors, for example,
220 accelerometers, pore pressure gauges, potentiometers and Laser Displacement Transducers
221 (LDT) are installed at different locations, as shown in Figs. 1 and 2. The sensors located inside
222 the ground are installed during the model ground preparation.

223

224 *2.3. Applied ground motions*

225 Two successive ground motions are applied to the model ground, as shown in Fig. 7. The
226 Japanese design specification for highway bridges [40] recommends the sustainability of the
227 highway bridges should be checked for Level-2 earthquakes. Therefore, the Tohoku ground
228 motion is applied to the model ground. The recorded acceleration at the base of the container
229 is similar to the real Tohoku Earthquake recorded at the ground surface near the New
230 Bansuikyo Bridge, Tochigi (2-I-I-3, NS component) which corresponds to Type I of Level-2
231 earthquake. Unfortunately, the magnitude is comparatively smaller. A comparison of the
232 spectral accelerations of the applied ground motions and the design spectra of Level-2
233 earthquake (2-I-I-3) is shown in Fig. 8. The figure shows that the applied Tohoku ground
234 motion is comparatively smaller than the design spectra. However, the first ground motion
235 applied to the model ground will be described as the Tohoku Earthquake in this paper.

236 Comparatively strong sinusoidal waves are applied in the second shaking as the first ground
237 motion is smaller in magnitude than the design earthquake. The frequency and the amplitude
238 of the sinusoidal waves are 1.42 Hz and 0.49 g, respectively. It is to be mentioned here that
239 the second ground motion is applied once the excess pore water pressure by the first ground
240 motion is completely dissipated. The Arias intensity [41] of the applied ground motions in all
241 the cases is compared in Fig. 9 to check the repeatability of the input motions in different
242 experimental cases and the difference in the applied energy to the model. The graphs show
243 that the Arias intensity of the input ground motions in all the cases is quite comparable.

244

245 **3. Test results and discussion**

246 The recorded data are presented and described in the prototype scale. The important
247 parameters include the propagation of the seismic wave, the evolution of excess pore water

pressure, associated ground deformation, displacement of the abutment and the induced bending moment on the piles.

3.1. Excess pore water pressure evolution

The generation of excess pore water pressure triggers the lateral spreading, which is augmented by the liquefaction of the soil inside the channel. Several pore pressure gauges are installed in the loose and the dense soil under the embankment slope (P2-3) and inside the river channel (P3-3 and P3-5) to monitor the evolution of excess pore water pressure. The soil is considered to be liquefied when the excess pore water pressure (Δu) reaches the initial vertical effective stress (σ_0'). The excess pore pressure ratio $r_{u,}$ which is estimated by the ratio of excess pore water pressure and the initial vertical effective stress ($\Delta u/\sigma_0'$) is another popular way to represent the soil liquefaction. The soil is considered as liquefied when the r_u at that location reaches 1.0.

The excess pore water pressure time histories in C-5 (abutment without sheet pile) and C-6 (abutment with sheet pile) under the slope (P2-3) and inside the channel (P3-3), and immediately below the liquefiable layer inside the river channel (P3-5) are shown in Fig. 10 and Fig. 11, respectively. The pore pressure gauge P2-3 is located right behind the abutment pile in C-5 and C-6. The graphs show namely the r_u values of the liquefiable layer inside the river channel (P3-3) reaches 1.0 at the early stage of shaking at about 71 s and 30 s during the Tohoku Earthquake and the sinusoidal waves, respectively. The soil at P3-5, located 3.5 m deep into the dense layer, almost reaches the liquefied state at about 85 s which is followed by a quick dissipation afterwards in the Tohoku Earthquake. Whereas, the soil at P3-5 gets liquefied for the sinusoidal waves. The soil at P2-3 doesn't liquefy during the Tohoku

271 Earthquake. However, the ground reaches the liquefied state nearly around 36 s for the
272 sinusoidal waves.

273 The evolution of the excess pore water pressure at the corresponding locations in the case of
274 the embankment without abutment and sheet pile (C-1) is shown in Fig. 12. The comparison
275 of the excess pore water pressure evolutions in the different cases reveals that the excess
276 pore water pressure at P3-5 in C-1, C-5, and C-6 is almost the same in the phase and magnitude.
277 The r_u value at P3-3 located in the liquefiable layer inside the river channel also reaches 1.0 in
278 all three cases.

279 The existence of structure is reported to affect the liquefaction potential of the soil near the
280 structure [42, 43]. Rollins and Seed [42] reported that the liquefaction potential of the soil
281 close to the structure could depend on the soil density and the type of structure and concluded
282 that the soil below the short-period and low rise building could exhibit high liquefaction
283 potential. Dash and Bhattacharya [43] reported that the excess pore water pressure
284 generation could be slower near the inclined piles. However, in our centrifuge experiments,
285 the excess pore water pressure is insignificantly influenced by the existence of the abutment.
286 The excess pore water pressure at P2-3 located near the abutment pile in the liquefiable layer
287 in C-5 and C-6 shows a similar trend as seen at the same location in the case without abutment
288 (C-1), though the fluctuation is rather large in the cases without structures (see Figs. 10 – 12).
289 The evolutions of excess pore water pressure in C-3 are not shown here, but they are also
290 comparable to the other cases.

291 The trend and the magnitude of the excess pore water pressure at P2-3 and P3-3 are
292 significantly different as shown in Figs. 10 – 12 although they are located at the same elevation
293 in the centrifuge experiment. The pore pressure gauge at P2-3 is located under the

294 embankment slope whereas, the pore pressure gauge at P3-3 is located inside the river
295 channel. The stress conditions at those two locations are potentially different. The soil at P2-
296 3 is subjected to a considerably large confining stress than the soils located at P3-3. The large
297 confining stress hinders the soil to reach the liquefied state which is also true for P1-3 [37].
298 Therefore, the soils at P3-3 gets liquefied at the early stage of shaking whereas, the soils at
299 P2-3 don't liquefy particularly in the Tohoku Earthquake. It is observed that the overall ground
300 responses in terms of excess pore water pressure evolution in all the experimental cases are
301 almost the same. It indicates that the structural elements have a minor influence on the
302 evolutions of excess pore water pressure as mentioned above. Besides, the experimental
303 observation shows that dense soil can also liquefy depending on the magnitude and duration
304 of the earthquake.

305

306 *3.2. Efficiency of sheet pile to mitigate the channel-ward movement of the ground and the*
307 *abutment*

308 The expected function of the sheet pile is to mitigate the channel-ward movement of the
309 ground. It is expected that the mitigation of the lateral spreading can reduce the channel-ward
310 movement of the abutment thus minimize the damage of the structure, such as piled
311 abutment associated with the lateral spreading. Two targets (TR-1 and TR-2) are placed on the
312 embankment slope to monitor the channel-ward movement of the ground, as shown in Figs.
313 1 and 2. The target TR-1 is located near the shoulder in C-1 and C-3 (the cases without
314 abutment), whereas, TR-1 corresponds to the abutment (2.0 m below the crest) in C-5 and C-
315 6. The target TR-2 is located in the middle of the embankment slope, where the sheet pile is
316 installed in C-3 and C-6.

317 Comparisons of the horizontal displacement at TR-1 and TR-2 in all the cases are shown in Fig.
318 13 for the Tohoku Earthquake and the sinusoidal waves. The comparison of the horizontal
319 displacement at TR-1 and TR-2 between reinforced and unreinforced cases with an abutment
320 (C-5 and C-6) shows that the reinforcement can considerably reduce the channel-ward ground
321 movement. Similarly, in C-1 and C-3, the horizontal displacement at TR-1 and TR-2 is also
322 significantly reduced with the installation of sheet pile. The horizontal displacement time
323 histories near the crest of the abutment (2 m below the crest) with and without the sheet pile
324 (C-5 and C-6) are shown in Fig. 14. The graphs clearly illustrate that the channel-ward
325 displacement of the abutment is reduced up to 41 % for the Tohoku Earthquake, which is
326 around 34 % for the sinusoidal waves. This observation certifies the efficiency of the sheet pile
327 as a seismic retrofit against the liquefaction-induced lateral spreading.

328 The channel-ward movement of the embankment, as well as the abutment, is caused by the
329 combined action of the propagated seismic energy to the embankment and the lateral
330 spreading of the loose foundation. The displacement vector of the model ground obtained
331 from PIV analysis [44] for C-1 shows clear evidence of lateral spreading [37]. The loose soil in
332 the embankment slope moves both vertically and horizontally during the earthquakes
333 whereas, the loose saturated foundation significantly moves towards the river channel.
334 Besides, the ground deformation is considerably large during the sinusoidal waves in
335 comparison with the Tohoku Earthquake since the input energy in sinusoidal waves is much
336 larger than the Tohoku Earthquake.

337 An attempt is made to quantify the channel-ward movement of the laterally spreading ground.
338 Several vertical coloured noodles are placed at the various locations shown in Fig. 15 to track
339 the ground movement after the shaking. The coloured noodles are placed immediately behind

340 the glass window to make the deformation visible from the outside of the container. The
341 deformation of the coloured noodles after the successive shakings is manually measured and
342 compared between the reinforced and unreinforced cases, as shown in Fig. 16. The coloured
343 noodles are placed 9 m behind the sheet pile (towards the backfill), 1 m and 6 m in front of
344 the sheet pile (towards the channel). Because of the build-up of excess pore water pressure
345 in the dense layer as seen at P3-5 (see Fig. 11 for C-6,) a certain deformation of the ground
346 takes place even in the dense layer, leading to the tilting of the sheet pile. However, the stiff
347 sheet pile can constrain the liquefied soil in the loose layer and make the distribution of the
348 horizontal displacement rather straight compared to the case without sheet pile (see the
349 displacement profile at a distance of 1 m towards channel from sheet pile.) As a result, the
350 ground deformation in the reinforced cases (C-3 and C-6) is significantly smaller than the
351 ground deformation in the unreinforced cases (C-1 and C-5). Therefore, the graphs clearly
352 illustrate the efficiency of the sheet pile to mitigate lateral spreading.

353 The ground deformation profiles in Fig. 16 and the horizontal displacement of the targets TR-
354 1 and TR-2 in Fig. 13 reveal that the channel-ward movement of the ground below the
355 abutment (or below the embankment slope in the case without abutment) is not affected by
356 the existence of the abutment but is controlled by the existence of the sheet pile. These
357 indicate that the piled abutment is almost following the movement of the ground. A
358 comparison of the displacement time histories at TR-2, which is at the top of the sheet pile in
359 C-3 (without abutment) and C-6 (with abutment), are shown in Fig. 17. This graph also shows
360 that the horizontal displacement of the sheet pile is almost the same irrespective to with or
361 without abutment. These clearly illustrate that the old piled abutment is relatively flexible as
362 compared to the sheet pile that has a minor pinning effect on the ground movement. Besides,
363 the channel-ward ground movement which is predominantly controlled by the sheet pile in

364 the reinforced cases, leading to the less rotation of the foundation in the reinforced cases as
365 will be described in the following sections. On the contrary, in the case with comparatively
366 stiff piles, marked pinning effect could be confirmed and such piles could attract more load
367 from laterally spreading soil [45].

368

369 *3.3. Bending moment response of sheet pile*

370 The sheet pile as a seismic retrofit carries a large amount of kinematic load imposed by the
371 laterally spreading soil and the embankment. The bending moment response of the sheet pile
372 provides the information regarding its contribution to carrying the load imposed by lateral
373 spreading. The sign convention used in this paper for the bending moment of the sheet pile is
374 shown in Fig. 18 (a). The bending moment that causes the curvature of the sheet pile concave
375 towards the river channel is considered as positive in this paper. A comparison of the bending
376 moment profiles of the sheet pile in C-3 (without abutment) and C-6 (with abutment) is shown
377 in Fig. 19 when the sheet pile experiences the maximum bending moment. The maximum
378 bending moment takes place around 86.0 s in Tohoku Earthquake and 48.0 s in sinusoidal
379 waves. The graph demonstrates that the bending moment profiles of the case with and
380 without abutment are comparable except the upper part (at a depth up to 4 m from the
381 surface of the foundation ground) of the sheet pile, particularly during the sinusoidal waves.
382 The difference in the bending moment profile is probably because of the interaction between
383 the abutment footing and the sheet pile. Apart from this minor difference, the bending
384 moment profiles are very similar in terms of shape and magnitude. It indicates that the
385 majority of the mobilized load from the laterally spreading soil is carried by the sheet pile

rather than the abutment piles. In another word, the ground deformation around the old piled abutment is mostly controlled by the sheet pile reinforcement.

3.4. Mitigation of bending moment of abutment piles

The abutment pile in laterally spreading soil can be damaged due to bending caused by the kinematic force from the soil and the inertia force from the abutment. The efficiency of the sheet pile to mitigate the pile bending moment is investigated in this section. Two piles are instrumented with strain gauges, as shown in Fig. 5 to record the bending strain during the experiment. The sign convention used for the bending moment of the piles is shown in Fig. 18 (b). The sign convention for piles is the same as the sign convention used for the sheet pile. The channel-ward concave curvature of the pile is considered as positive bending.

The bending moment profiles of Pile-1 and Pile-2 (see Fig. 2) in C-5 (without sheet pile) and C-6 (with sheet pile) are shown in Fig. 20 when the piles experience the maximum bending moment. Pile-1_5 in Fig. 20 represents the bending moment profile of Pile-1 in C-5. Similarly, Pile-2_5, Pile-1_6 and Pile-2_6 represent Pile-2 in C-5, Pile-1 in C-6, and Pile-2 in C-6, respectively. The two piles do not necessarily experience the maximum bending at the same time. For example, Pile-1 and Pile-2 experience maximum bending moment both at 86.83 s during Tohoku Earthquake whereas, during the sinusoidal waves Pile-1 experiences the maximum bending moment at 49.59 s and Pile-2 experiences the maximum bending moment at 49.52 s. However, the piles most of the cases experience maximum bending moment almost at the end of the effective shaking. The bending moment distributions in Fig. 20 show that the piles exhibit different response due to the existence of sheet pile reinforcement. The piles in the reinforced case (C-6) experience maximum bending moment near its head, whereas, the

maximum bending moment is observed near the interface of the loose and the dense layer in the unreinforced case (C-5). This tendency is clearly seen for the Tohoku Earthquake.

The alteration of the pile response in the reinforced case is probably because of the change in the ground displacement profile around the piles and the limited rotation of the pile. The latter will be described in the next subsection. This largely influences kinematic load from the soils. The existence of the sheet pile alters the ground displacement profile around the abutment piles as explained in Subsection 3.2. The sheet pile erases the large change in the horizontal displacement around the interface between the loose and dense layers. This contributes to the significant reduction of the bending moment around the interface. The smaller channel-ward displacement of the abutment in the reinforced case decrease the bending moment near the pile heads. Besides, because of the frame formed with the footing and piles, the movement of the abutment is translational and hence the reduction of the bending moment around the interface also contributes to the reduction of the bending moment near the pile heads. As a result, the reduction of the bending moment is nearly around 40 % near the pile head and the interface of the loose and the dense layer as well. It should be noted that the bending moment near the pile heads (at a depth of 2 m from the ground surface) cannot be measured during the sinusoidal waves in the unreinforced case (C-5) because of the malfunctioning of the strain gauges.

The bending moment near the pile head is caused by the combined action of the kinematic load from the soils and the inertia force of the abutment. The effect of inertia force on the pile bending moment gradually decreases with depth. The time histories of the bending moment near the head of the Pile-1 and Pile-2 (at a depth of 0.25 m) along with the horizontal displacement at TR-1 (2.0 m below the crest of the abutment) and acceleration of the

abutment footing (A-ft) in C-6 (with sheet pile) are shown in Fig. 21 to observe the contribution of the inertia force of the abutment. The maximum bending moment appears just after the principal shock. The maximum bending moment takes place at 86.83 s in the Pile-1 and Pile-2 during the Tohoku Earthquake. Whereas, the peak acceleration of the abutment is recorded at 84.27 s. The bending moment is observed to increase with the increasing channel-ward movement of the abutment even after the principal shock. This indicates that the maximum bending moment does not necessarily coincide with the event of peak acceleration of the abutment and is predominantly guided by the lateral spreading of the ground. Therefore, simultaneous application of the inertia force using peak acceleration and the kinematic effect induced by the lateral spreading in the design calculation for piled abutment might yield a rather conservative result.

3.5. Deformation mode of abutment piles

If we ignore the strut effect of the bridge girder as in this experiment, a piled abutment is expected to show the translational movement because of the frame formed with the footing and piles. In this type of deformation pattern, the bending stress in a pile arises due to the excessive translation of the comparatively rigid footing. The deformed shape of the pile provides an idea about the failure mechanism of the pile in this type of deformation pattern. The deformed shape of Pile-1 and Pile-2 along with the deformed shape of the abutment is plotted in Fig. 22 when the piles experience the maximum bending moment during the Tohoku Earthquake. The deformed shape is calculated from the bending moment recorded during the experiment. The simple area-moment method of beam deflection is used here to estimate the pile displacement. In the calculation, it is assumed that (1) the pile heads have equal

translational displacement as they are connected to the rigid footing and (2) the horizontal movement of the pile tips is considered as zero. As for the second boundary condition, the pile tips are free to move in reality. However, as the magnitude of the displacement at the pile tip is negligibly small in comparison with the pile head displacement, this assumption is applied in the calculation.

The deformed shape of the piles and the abutment without reinforcement (C-5) shows that the piles go under significant rotation at the interface of the loose and dense layer without causing any major tilting of the abutment. The rotation of the pile is around 5°. This excessive rotation of the pile without any significant tilting of the abutment increases the bending stress near the pile head and the interface of the loose and the dense layer. The installation of the sheet pile reduces the kinematic load acting on the piles and the translational movement of the abutment thus significantly reduce the rotation of the pile as shown in Fig. 22 (b). The rotation of the pile is reduced to 2.5° in the reinforced case, resulting in a significant reduction of the bending stress at the pile head and the interface. The installation of the sheet pile without any direct connection to the abutment does not change the deformation pattern of the piles but could mitigate excessive displacement of the abutment and pile bending moment.

4. Conclusions

A series of dynamic centrifuge experiments are conducted to investigate (1) the deformation pattern of the old piled abutment subjected to liquefaction-induced lateral spreading and (2) the performance of the sheet pile to mitigate the damage of the abutment piles due to lateral spreading. The experimental results are also compared with the cases without abutment

having similar geometric configurations to study the pinning effect of the piled abutment against the lateral spreading of the ground.

The experimental results reveal that the old piled abutment moves together with the spreading soil and shows channel-ward translational movement without pinning effect. The piles experience the large bending moment around the pile head and the interface between the loose and dense layers due to the lateral spreading of the ground as expected. The sheet pile with sufficient embedment depth can reduce the channel-ward movement of the abutment up to 40% thus helps to minimize the bending stress on the supporting piles. The sheet pile is found effective in mitigating the channel-ward movement of the abutment thus mitigate the bending moment demand of the piles under moderate to strong ground motion.

Since the old piled abutments are comparatively flexible, it exhibits minor pinning effect against the lateral spreading and consequently flows with the liquefied ground. The lateral spreading of the ground predominantly guides the maximum bending moment of the piles. Because of this, the bending moment is observed to increase with the increasing channel-ward movement of the embankment slope even after the principal shock. Therefore, simultaneous application of the inertia force using peak acceleration and the kinematic effect induced by the lateral spreading in the design calculation for piled abutment might yield a rather conservative result.

It is worth noting that the seismic response of the soil-structure system might differ with the soil stratification, ground geometry, type of structure and seismic excitation. Therefore, the results described in this paper cannot be generalized for other types of abutment system. Further studies with various soil and structural configurations are needed to come to any generalized conclusion.

Acknowledgements

This study was supported by the research grant from the Japan Iron and Steel Federation in FY2019-2020. The first author would like to acknowledge the financial support provided by Monbukagakusho (Ministry of Education, Culture, Sports, Science and Technology) scholarship during his study in Japan. The authors are also indebted to Mr Sakae Seki for his continuous cooperation during the centrifuge experiments.

References

[1] Hamada M, O'Rourke TD. Case studies of liquefaction and lifeline performance during past earthquakes, Vol. 1 Japanese case studies. Natl Cent Earthq Eng Res Tech Rep 1992;1:422.

[2] Tokimatsu K, Mizuno H, Kakurai M. Building damage associated with geotechnical problems. Soils Found 1996:219–34. https://doi.org/10.3208/sandf.36.special_219.

[3] Tokimatsu K, Asaka Y. Effects of liquefaction-induced ground displacements on pile performance in the 1995 Hyogoken-Nambu earthquake. Soils Found 1998;38:163–77. https://doi.org/10.3208/sandf.38.special_163.

[4] Abdoun T, Dobry R, O'Rourke TD, Goh SH. Pile response to lateral spreads: Centrifuge modeling. J Geotech Geoenvironmental Eng 2003;129:869–78. https://doi.org/10.1061/(ASCE)1090-0241(2003)129:10(869).

[5] Knappett JA, Mohammadi S, Griffin C. Lateral spreading forces on bridge piers and pile caps in laterally spreading soil: Effect of angle of incidence. J Geotech

Geoenvironmental Eng 2010;136:1589–99. https://doi.org/10.1061/(ASCE)GT.1943-5606.0000387.

[6] Youd TL. Liquefaction-induced damage to bridges. Transp Res Rec 1993:35–41.

[7] Bartlett SF. Liquefaction-induced ground failure and bridge damage to the Alaskan railroad and highway in South Central Alaska during the 1964 Alaskan Earthquake. Proc. 10th Natl. Conf. Earthq. Eng. Anchorage, AK, Earthquake Engineering Research Institute; 2014.

[8] Waldin J, Jennings J, Routledge P. Critically damaged bridges & concepts for earthquake recovery. Proc. New Zeal. Soc. Earthq. Eng. Annu. Conf., 2012, p. 1–8.

[9] Haskell JJM, Madabhushi SPG, Cubrinovski M, Winkley A. Lateral spreading-induced abutment rotation in the 2011 Christchurch earthquake: Observations and analysis. Geotechnique 2013;63:1310–27. https://doi.org/10.1680/geot.12.P.174.

[10] Mohanty P, Bhattacharya S. Case Studies of Liquefaction-Induced Damages to Two Pile-Supported River Bridges in China. J Perform Constr Facil 2019;33. https://doi.org/10.1061/(ASCE)CF.1943-5509.0001306.

[11] Berrill JB, Christensen SA, Keenan RP, Okada W, Pettinga JR. Case study of lateral spreading forces on a piled foundation. Geotechnique 2001;51:501–17. https://doi.org/10.1680/geot.2001.51.6.501.

[12] Finn WDL, Fujita N. Piles in liquefiable soils: seismic analysis and design issues. Soil Dyn Earthq Eng 2002;22:731–42. https://doi.org/10.1016/S0267-7261(02)00094-5.

[13] Ebeido A, Elgamal A, Tokimatsu K, Abe A. Pile and Pile-Group Response to Liquefaction-Induced Lateral Spreading in Four Large-Scale Shake-Table Experiments. J Geotech

544 Geoenvironmental Eng 2019;145. https://doi.org/10.1061/(ASCE)GT.1943-
545 5606.0002142.

546 [14] Liu C, Tang L, Ling X, Deng L, Su L, Zhang X. Investigation of liquefaction-induced lateral
547 load on pile group behind quay wall. Soil Dyn Earthq Eng 2017;102:56–64.
548 https://doi.org/10.1016/j.soildyn.2017.08.016.

549 [15] Yasuda S, Ishihara K, Morimoto I, Orense R, Ikeda M, Tamura S. Large-scale shaking
550 table tests on pile foundations in liquefied ground. 12th World Conf Earthq Eng
551 2000:Paper No. 1474.

552 [16] Kavand A, Haeri SM, Asefzadeh A, Rahmani I, Ghalandarzadeh A, Bakhshi A. Study of
553 the behavior of pile groups during lateral spreading in medium dense sands by large
554 scale shake table test. Int J Civ Eng 2014;12:374–91.

555 [17] Wang X, Ji B, Ye A. Seismic Behavior of Pile-Group-Supported Bridges in Liquefiable Soils
556 with Crusts Subjected to Potential Scour: Insights from Shake-Table Tests. J Geotech
557 Geoenvironmental Eng 2020;146. https://doi.org/10.1061/(ASCE)GT.1943-
558 5606.0002250.

559 [18] Motamed R, Towhata I, Honda T, Tabata K, Abe A. Pile group response to liquefaction-
560 induced lateral spreading: E-Defense large shake table test. Soil Dyn Earthq Eng
561 2013;51:35–46. https://doi.org/10.1016/j.soildyn.2013.04.007.

562 [19] Brandenberg SJ, Boulanger RW, Kutter BL, Chang D, et al. Behavior of pile foundations
563 in laterally spreading ground during centrifuge tests. J Geotech Geoenvironmental Eng
564 2005;131(11):1378–91. https://doi.org/10.1061/(ASCE)1090-0241(2005)131:11(1378).

565 [20] Takahashi A, Sugita H, Tanimoto S. Centrifuge model tests on abutments of river-

crossing bridge on liquefiable soils. 4th Int. Conf. Earthq. Geotech. Eng. Pap. ID 1618, 2007.

[21] Takahashi A, Sugita H, Tanimoto S. Forces acting on bridge abutments over liquefied ground. Soil Dyn Earthq Eng 2010;30:146–56. https://doi.org/10.1016/j.soildyn.2009.10.007.

[22] Saha P, Takahashi A. Seismic performance of pile-supported bridge abutment resting on a liquefiable soil layer. 3rd Int. Conf. Performance-based Des. Earthq. Geotech. Eng. Pap. ID 504, 2017.

[23] Saha P, Horikoshi K, Takahashi A. 3D Numerical simulation of old pile-supported bridge abutment subjected to lateral spreading. 53rd Japan Natl. Conf. Geotech. Eng. Pap. ID 930, 2018.

[24] Saha P, Horikoshi K, Takahashi A. Effectiveness of sheet pile as a seismic retrofit for piled abutment subjected to liquefaction-induced lateral spreading. Earthq. Geotech. Eng. Prot. Dev. Environ. Constr. Proc. 7th Int. Conf. Earthq. Geotech. Eng., 2019, p. 4784–91.

[25] Japan Road Association. Design guideline of substructures for highway bridges (Design of pile foundations), 1964.

[26] Liu L, Dobry R. Seismic response of shallow foundation on liquefiable sand. J Geotech Eng 1997;123:557–66. https://doi.org/10.1061/(asce)1090-0241(1997)123:6(557).

[27] Adalier K, Elgamal AW, Martin GR. Foundation liquefaction countermeasures for earth embankments. J Geotech Geoenvironmental Eng 1998;124:500–17. https://doi.org/10.1061/(ASCE)1090-0241(1998)124:6(500).

588 [28] Okamura M, Matsuo O. Effects of remedial measures for mitigating embankment
589 settlement due to foundation liquefaction. Int J Phys Model Geotech 2002;2:01–12.
590 https://doi.org/10.1680/ijpmg.2002.020201.

591 [29] Adalier K, Aydingun O. Numerical analysis of seismically induced liquefaction in earth
592 embankment foundations. Part II. Application of remedial measures. Can Geotech J
593 2003;40:766–79. https://doi.org/10.1139/t03-026.

594 [30] Watanabe T. Damage to oil refinery plants and a building on compacted ground by the
595 Niigata earthquake and their restoration. Soils Found 1966;6:86–99.
596 https://doi.org/10.3208/sandf1960.6.2_86.

597 [31] Ishihara K, Kawase Y, Nakajima M. Liquefaction Characteristics of Sand Deposits at an
598 Oil Tank Site During The 1978 Miyagiken-Oki Earthquake. Soils Found 1980;20:97–111.
599 https://doi.org/10.3208/sandf1972.20.2_97.

600 [32] Yasuda S, Harada K, Ishikawa K, Kanemaru Y. Characteristics of liquefaction in Tokyo
601 Bay area by the 2011 Great East Japan Earthquake. Soils Found 2012;52:793–810.
602 https://doi.org/10.1016/j.sandf.2012.11.004.

603 [33] Pamuk A, Gallagher PM, Zimmie TF. Remediation of piled foundations against lateral
604 spreading by passive site stabilization technique. Soil Dyn Earthq Eng 2007;27:864–74.
605 https://doi.org/10.1016/j.soildyn.2007.01.011.

606 [34] Motamed R, Towhata I. Mitigation measures for pile groups behind quay walls
607 subjected to lateral flow of liquefied soil: Shake table model tests. Soil Dyn Earthq Eng
608 2010;30:1043–60. https://doi.org/10.1016/j.soildyn.2010.04.016.

609 [35] Takemura J, Kondoh M, Esaki T, Kouda M, Kusakabe O. Centrifuge model tests on

610 double propped wall excavation in soft clay. Soils Found 1999;39:75–87.
611 https://doi.org/10.3208/sandf.39.3_75.

612 [36] Iai S, Tobita T, Nakahara T. Generalised scaling relations for dynamic centrifuge tests.
613 Geotechnique 2005;55:355–62. https://doi.org/10.1680/geot.2005.55.5.355.

614 [37] Saha P, Horikoshi K, Takahashi A. Performance of sheet pile to mitigate liquefaction-
615 induced lateral spreading of loose soil layer under the embankment. Soil Dyn Earthq
616 Eng 2020;139:106410. https://doi.org/10.1016/j.soildyn.2020.106410.

617 [38] Chopra AK. Dynamics of Structures: Theory and Applications to Earthquake Engineering.
618 Fourth. Pearson Education; 2012.

619 [39] Adamidis O, Madabhushi GSP. Use of viscous pore fluids in dynamic centrifuge
620 modelling. Int J Phys Model Geotech 2015;15:141–9.
621 https://doi.org/10.1680/ijpmg.14.00022.

622 [40] Japan Road Association. Specifications for highway bridges-Part V seismic design, Tokyo,
623 Japan, 2014.

624 [41] Arias A. A measure of earthquake intensity. Seism. Des. Nucl. Power Plants, MIT Press;
625 1970, p. 438–83.

626 [42] Rollins KM, Seed HB. Influence of buildings on potential liquefaction damage. J Geotech
627 Eng 1990;116:165–85. https://doi.org/10.1061/(ASCE)0733-9410(1990)116:2(165).

628 [43] Dash SR, Bhattacharya S. Pore water pressure generation and dissipation near to pile
629 and far-field in liquefiable soils. Int J GEOMATE 2015;9:1454–9.
630 https://doi.org/10.21660/2015.18.4253.

631 [44] White DJ, Take W a. GeoPIV: Particle Image Velocimetry (PIV) software for use in
632 geotechnical testing. Cambridge Univ Eng Dep Tech Rep 2002:15.

633 [45] Armstrong RJ, Boulanger RW, Beaty MH. Liquefaction effects on piled bridge
634 abutments: Centrifuge tests and numerical analyses. J Geotech Geoenvironmental Eng
635 2013;139:433–43. https://doi.org/10.1061/(ASCE)GT.1943-5606.0000780.

636

List of Table captions:

Table 1: Test conditions.

Table 2: Scaling factor for different parameters used in the experiments assuming $\lambda_\varepsilon = 1.0$ [33].

Table 3: Physical properties of Toyoura sand.

Table 4: Specifications of the model abutment.

Table 5: Specifications of the pile foundation.

Table 6: Specifications of the sheet pile in model scale and prototype.

List of figure captions:

Fig. 1: Plan and cross-sectional views of the experimental setup; a) C-1 and b) C-3 (all the dimensions are in mm in model scale).

Fig. 2: Plan and cross-sectional views of the experimental setup; a) C-5 and b) C-6 (all the dimensions are in mm in model scale).

Fig. 3: Concept of simplification of the 3×4 piled abutment to the 2×2 piled abutment.

Fig. 4: Plan and cross-sections of the model abutment (all the dimensions are in mm in model scale).

Fig. 5: Acrylic pile used in the centrifuge experiment and the instrumentation with strain gauges (the dimensions are in model scale).

Fig. 6: Instrumentation of sheet pile (the dimensions are in mm in model scale).

657 Fig. 7: Input ground motions; a) Tohoku Earthquake and b) sinusoidal waves.

658 Fig. 8: Comparison of the design spectra of Level-2 earthquake and the spectral acceleration
659 of the applied ground motions.

660 Fig. 9: Comparison of the Arias intensity of the applied ground motions in all the cases; a)
661 Tohoku earthquake and b) sinusoidal waves.

662 Fig. 10: Excess pore water pressure time histories at P2-3, P3-3, and P3-5 in C-5 during Tohoku
663 Earthquake (left column) and sinusoidal waves (right column).

664 Fig. 11: Excess pore water pressure time histories at P2-3, P3-3, and P3-5 in C-6 during Tohoku
665 Earthquake (left column) and sinusoidal waves (right column).

666 Fig. 12: Excess pore water pressure time histories at P2-3, P3-3, and P3-5 in C-1 during Tohoku
667 Earthquake (left column) and sinusoidal waves (right column).

668 Fig. 13: Comparisons of the horizontal displacement at TR-1 and TR-2 in all the cases; a)
669 Tohoku Earthquake and b) sinusoidal waves.

670 Fig. 14: Comparisons of the horizontal displacement time histories near the crest (2.0 m below
671 the crest) of the abutment in C-5 and C-6; a) Tohoku Earthquake and b) sinusoidal waves.

672 Fig. 15: Locations of the abutment, sheet pile and the vertical noodles in the experimental
673 model.

674 Fig. 16: Deformation profiles of the foundation ground at different distances from the sheet
675 pile after the application of Tohoku Earthquake and sinusoidal waves.

676 Fig. 17: Comparisons of the horizontal displacement time histories at TR-2 in C-3 and C-6; a)
677 Tohoku Earthquake and b) sinusoidal waves.

678 Fig. 18: Sign convention used in this paper; a) sheet pile and b) abutment pile.

679 Fig. 19: Comparisons of the bending moment profiles of sheet pile in C-3 and C-6 when sheet
680 pile experiences the maximum bending moment; a) Tohoku Earthquake and b) sinusoidal
681 waves.

682 Fig.20: Bending moment profiles for Pile-1 and Pile-2 in C-5 and C-6 when the piles experience
683 the maximum bending moment.

684 Fig. 21: Time histories of bending moment near the head of the Pile-1 and Pile-2 (at a depth
685 of 0.25 m), horizontal displacement at TR-1 (2.0 m below the crest of the abutment) and
686 acceleration of the abutment footing (A-ft) in C-6.

687 Fig. 22: Displacement profiles of Pile-1 and Pile-2 along with the abutment in a) C-5 (without
688 sheet pile) and b) C-6 (with sheet pile) when the piles experience the maximum bending
689 moment during Tohoku Earthquake.

690

691 **Tables:**

692 Table 1: Test conditions.

Test ID	Existence of piled abutment	Width of abutment (m)	Existence of sheet pile	Width of sheet pile (m)	Relative density (%)		
					Embankment	Loose foundation	Dense foundation
C-1	No	No	No	-	54	53	92
C-3	No	No	Yes	Full-width	54	50	90
C-5	Yes	5	No	-	53	52	91
C-6	Yes	5	Yes	5 (in front of abutment)	54	51	94

693

694 Table 2: Scaling factor for different parameters used in the experiments assuming $\lambda_\varepsilon = 1.0$ [36].

Quantity	Model/Prototype
Length	$1/(50 \times 2) = 1/100$
Acceleration	$(50 \times 1) = 50$
Displacement	$1/(50\times2) = 1/100$
Time (dynamic)	$1/(50 \times 2^{0.5}) = 1/70.71$
Frequency	$50 \times 20^{0.5} = 70.71$
Bending stiffness, EI (structure)	$1/(50^4 \times 2^5) = 5 \times 10^{-9}$
Stress	1/2

695

696 Table 3: Physical properties of Toyoura sand.

Parameter	Value
Specific gravity	2.65
Maximum void ratio	0.973
Minimum void ratio	0.609
Mean diameter, D_{50} (mm)	0.19
Uniformity coefficient, C_u	1.32
Coefficient of permeability (Dr = 50%) (m/s)	2×10^{-4}
Coefficient of permeability (Dr = 90%) (m/s)	1×10^{-4}

697

698 Table 4: Specifications of the model abutment.

	Model	Prototype
Material type	Aluminium	Reinforced concrete
Length	50 mm	5 m
Width	50 mm	5 m
Height	80 mm	8 m
Weight (kN)	1.74×10^{-3}	1.74×10^{3}
Height of gravity centre (from base)	26 mm	2.6 m

699

700 Table 5: Specifications of the pile foundation.

	Model	Prototype
Material type	Acrylic	Reinforced concrete
Length	220 mm	22 m
Number of piles in half section	2 x 2	3 x 4
Sectional dimensions (mm)	4.75 × 10	360
Modulus of Elasticity (N/m2)	3.14×10^{9}	2.3×10^{10}
Bending stiffness of pile, EI (N-m^2)	0.28	1.9×10^{7}

701

702 Table 6: Specifications of the sheet pile in model scale and prototype.

	Model	Prototype
Material type	Steel	Steel
Bending stiffness, EI (N-m^2/m)	2.6×10^{2}	5.2×10^{8}
Target sheet pile	-	Hat-type & H-shape composite

703

704 **Figures:**

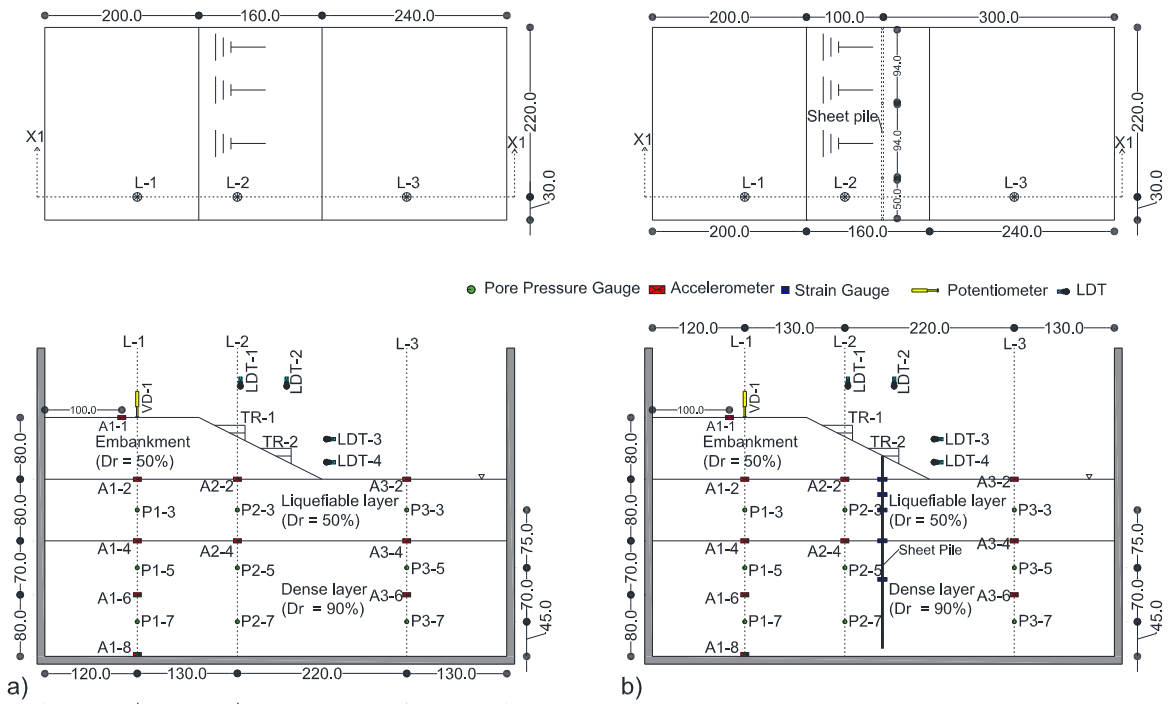

705

706 Fig. 1: Plan and cross-sectional views of the experimental setup; a) C-1 and b) C-3 (all the

707 dimensions are in mm in model scale).

708

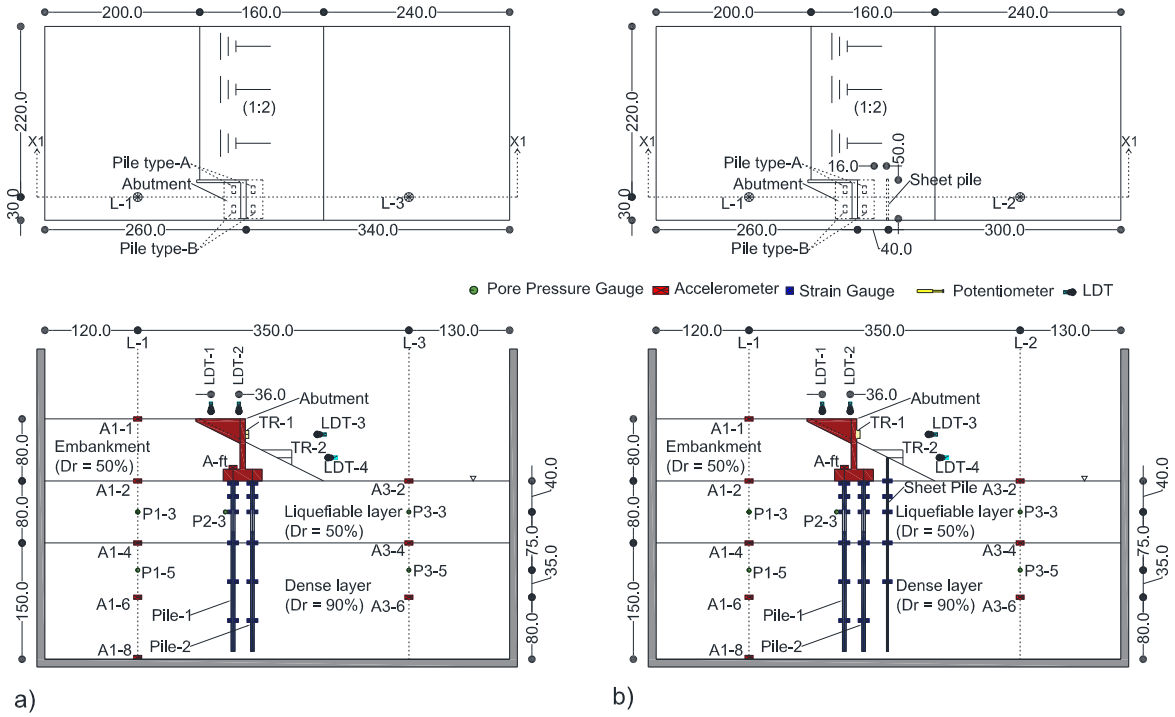

709

710 Fig. 2: Plan and cross-sectional views of the experimental setup; a) C-5 and b) C-6 (all the

711 dimensions are in mm in model scale).

712

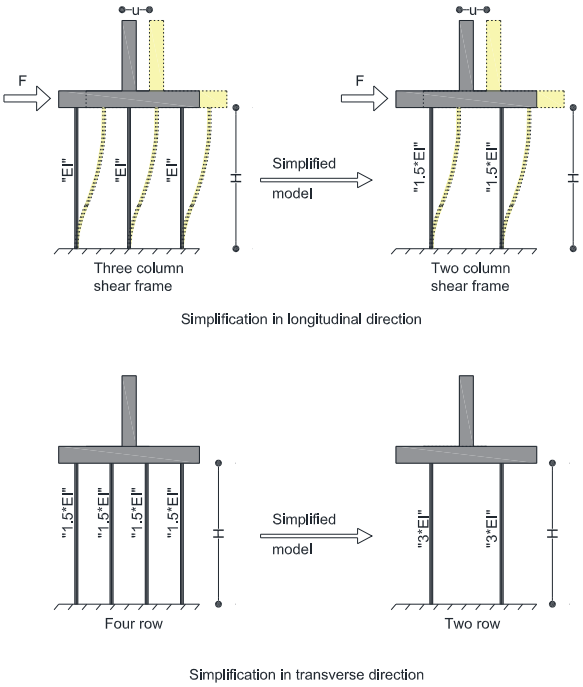

714

715 Fig. 3: Concept of simplification of the 3×4 piled abutment to the 2×2 piled abutment.

716

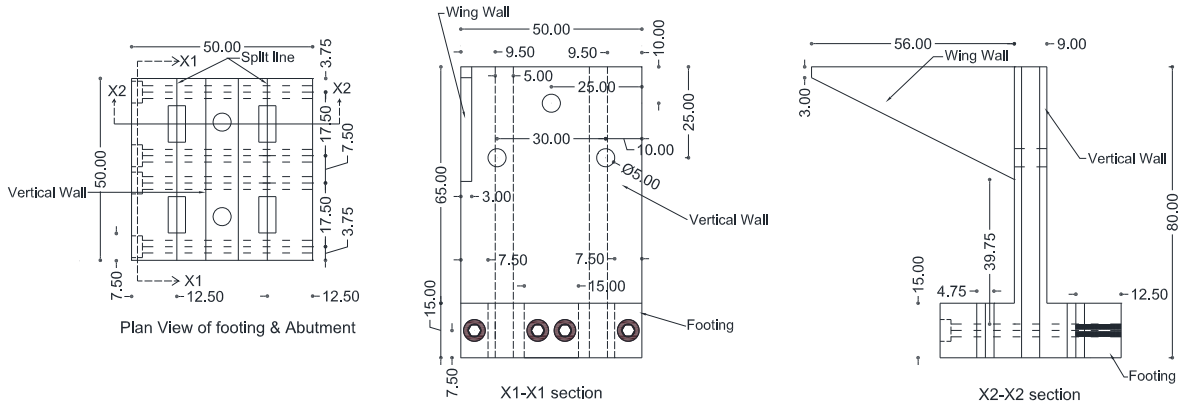

717

718 Fig. 4: Plan and cross-sections of the model abutment (all the dimensions are in mm in model

719 scale).

720

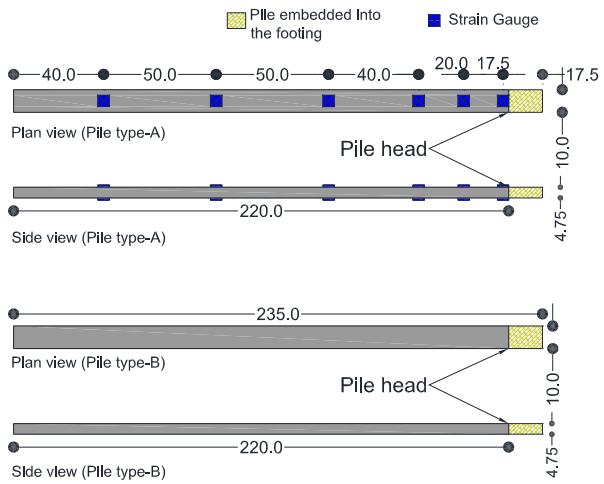

721

722 Fig. 5: Acrylic pile used in the centrifuge experiment and the instrumentation with strain

723 gauges (the dimensions are in model scale).

724

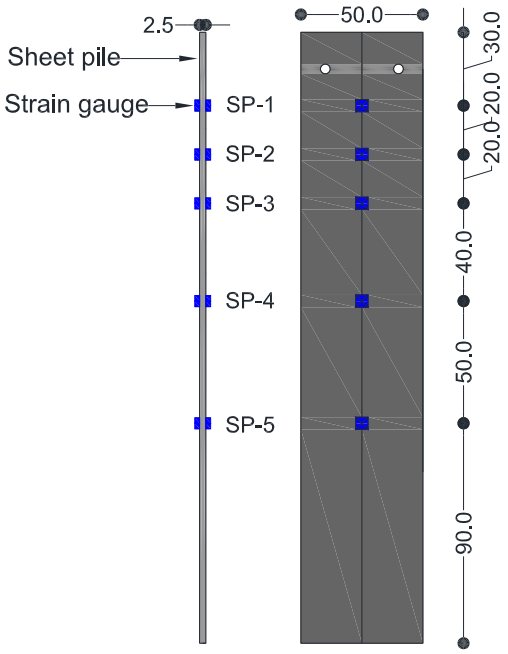

725

726 Fig. 6: Instrumentation of sheet pile (the dimensions are in mm in model scale).

727

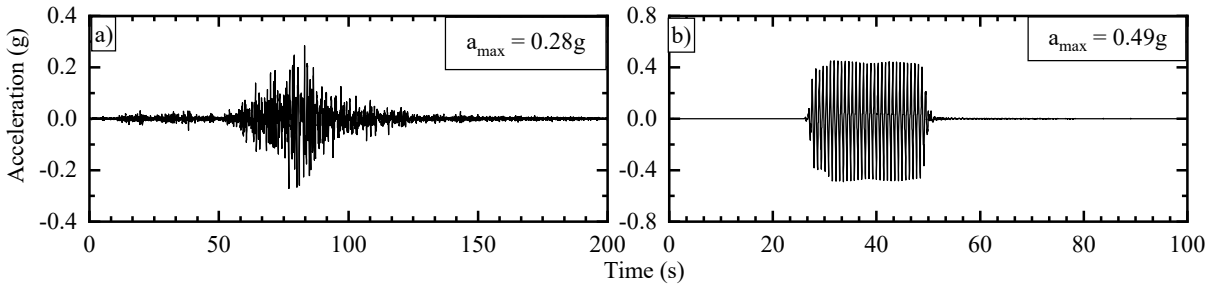

728

729 Fig. 7: Input ground motions; a) Tohoku Earthquake and b) sinusoidal waves.

730

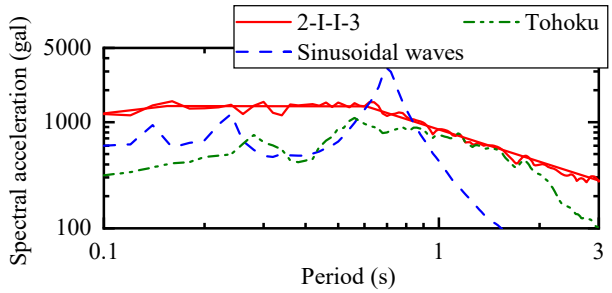

731

732 Fig. 8: Comparison of the design spectra of Level-2 earthquake and the spectral acceleration

733 of the applied ground motions.

734

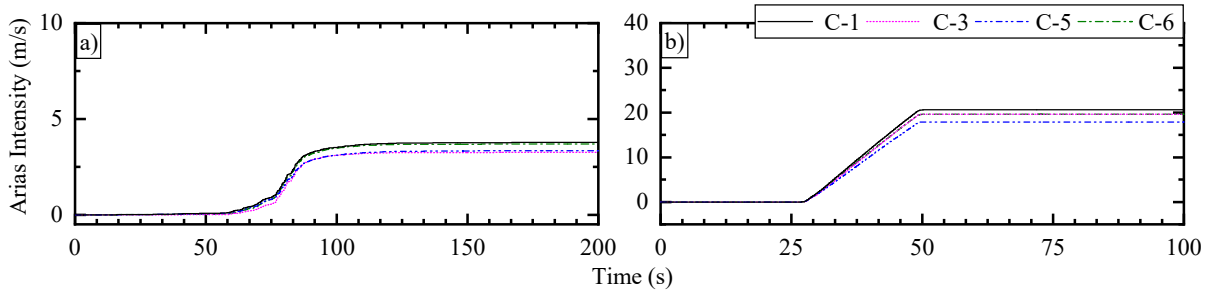

735

736 Fig. 9: Comparison of the Arias intensity of the applied ground motions in all the cases; a)

737 Tohoku earthquake and b) sinusoidal waves.

738

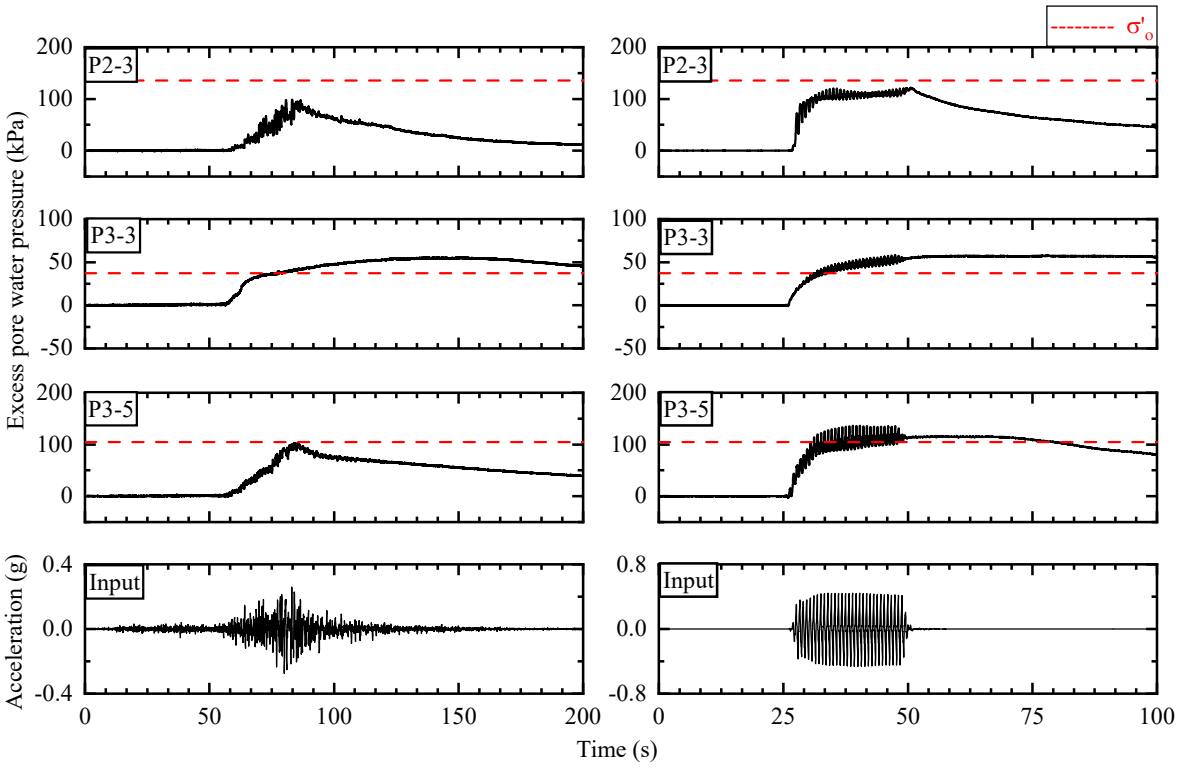

739

740 Fig. 10: Excess pore water pressure time histories at P2-3, P3-3, and P3-5 in C-5 during Tohoku

741 Earthquake (left column) and sinusoidal waves (right column).

742

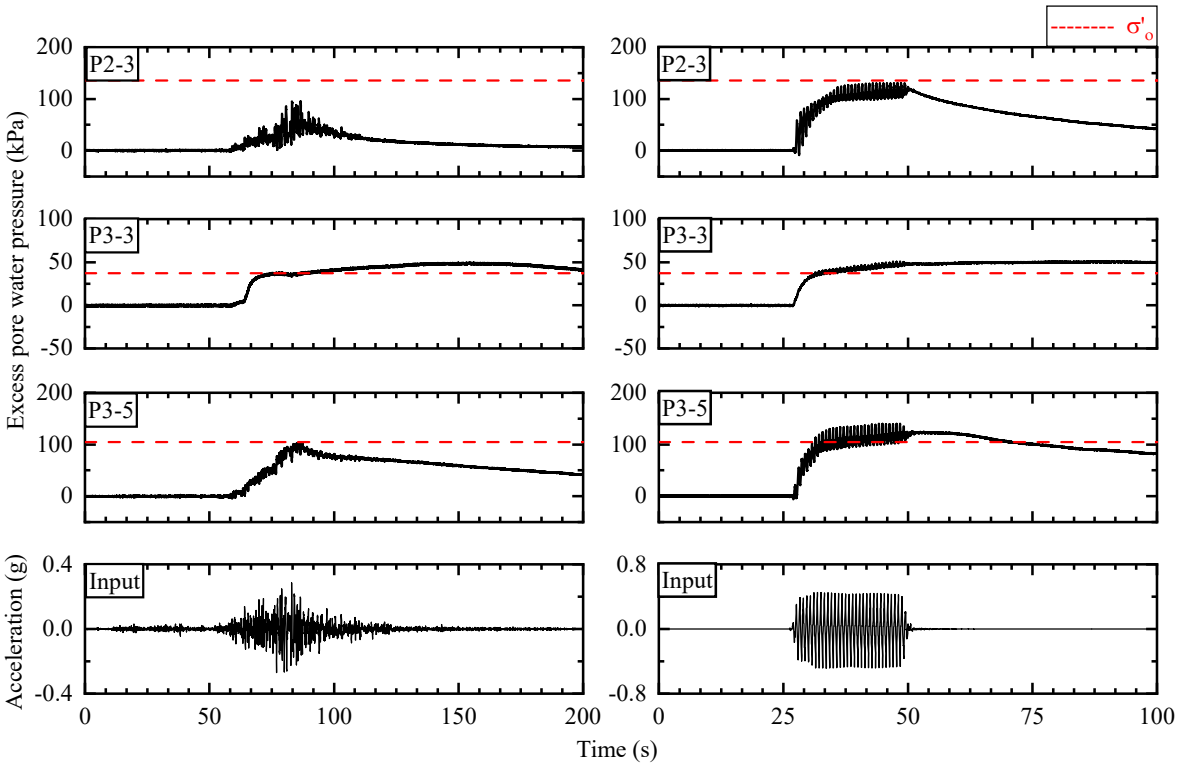

743

744 Fig. 11: Excess pore water pressure time histories at P2-3, P3-3, and P3-5 in C-6 during Tohoku

745 Earthquake (left column) and sinusoidal waves (right column).

746

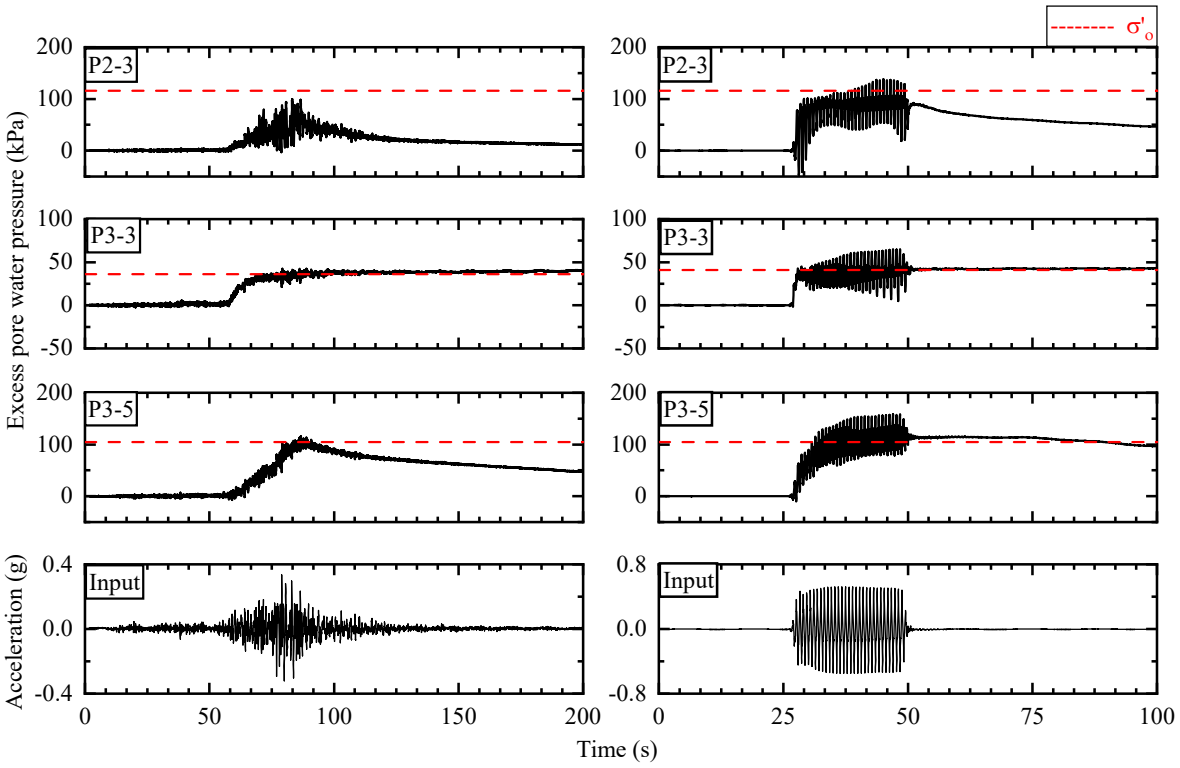

747

748 Fig. 12: Excess pore water pressure time histories at P2-3, P3-3, and P3-5 in C-1 during Tohoku

749 Earthquake (left column) and sinusoidal waves (right column).

750

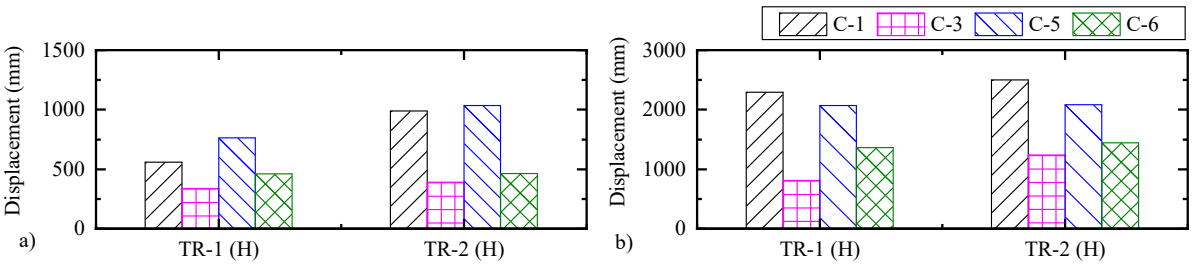

751

752 Fig. 13: Comparisons of the horizontal displacement at TR-1 and TR-2 in all the cases; a)

753 Tohoku Earthquake and b) sinusoidal waves.

754

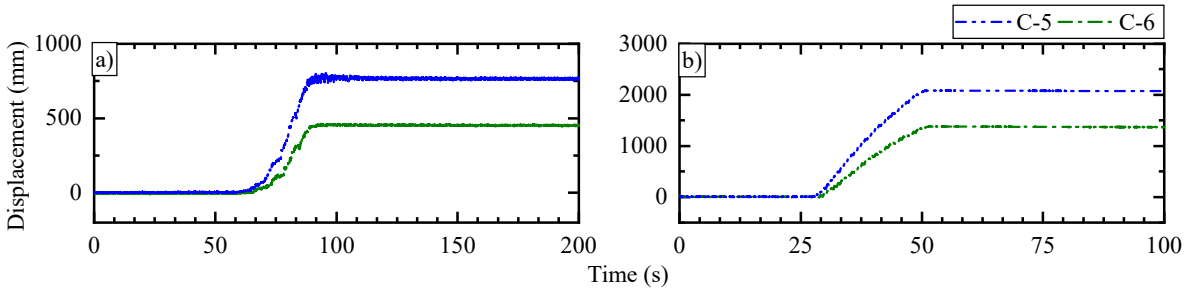

755

756 Fig. 14: Comparisons of the horizontal displacement time histories near the crest (2.0 m below

757 the crest) of the abutment in C-5 and C-6; a) Tohoku Earthquake and b) sinusoidal waves.

758

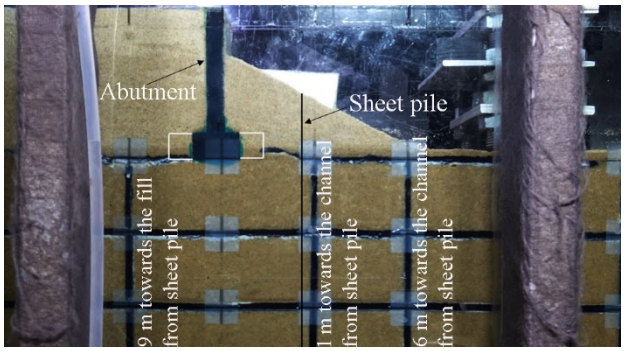

759

760 Fig. 15: Locations of the abutment, sheet pile and the vertical noodles in the experimental

761 model.

762

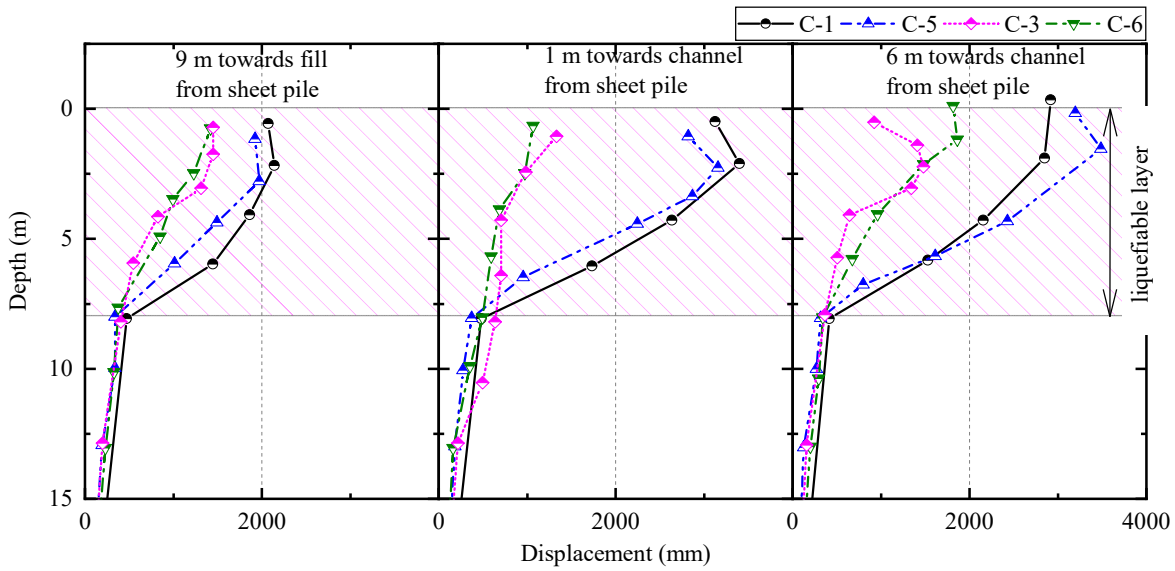

763

764 Fig. 16: Deformation profiles of the foundation ground at different distances from the sheet

765 pile after the application of Tohoku Earthquake and sinusoidal waves.

766

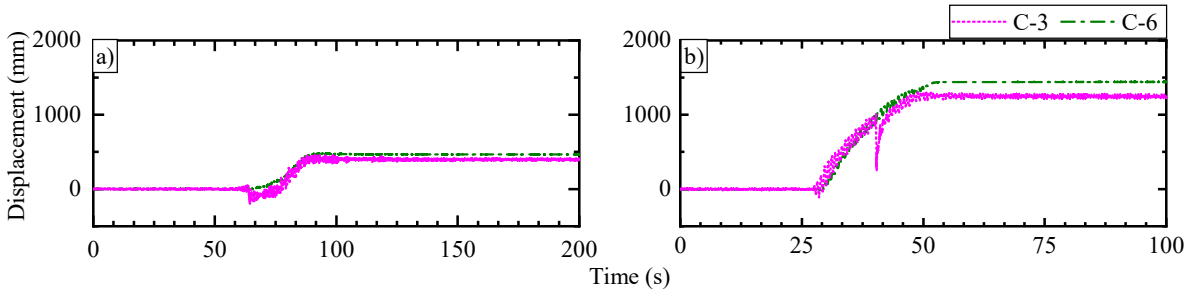

767

768 Fig. 17: Comparisons of the horizontal displacement time histories at TR-2 in C-3 and C-6; a)

769 Tohoku Earthquake and b) sinusoidal waves.

770

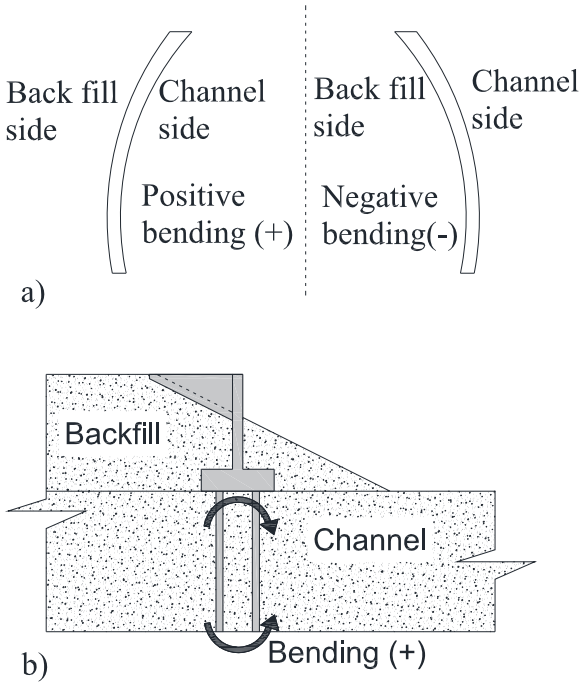

771

772 Fig. 18: Sign convention used in this paper; a) sheet pile and b) abutment pile.

773

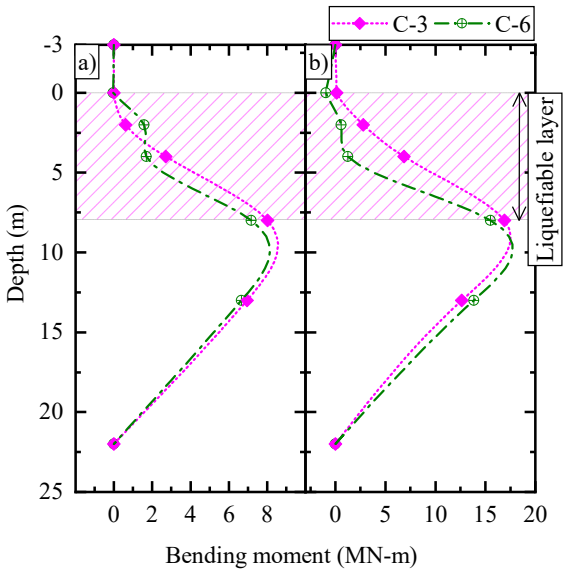

774

775 Fig. 19: Comparisons of the bending moment profiles of sheet pile in C-3 and C-6 when sheet

776 pile experiences the maximum bending moment; a) Tohoku Earthquake and b) sinusoidal

777 waves.

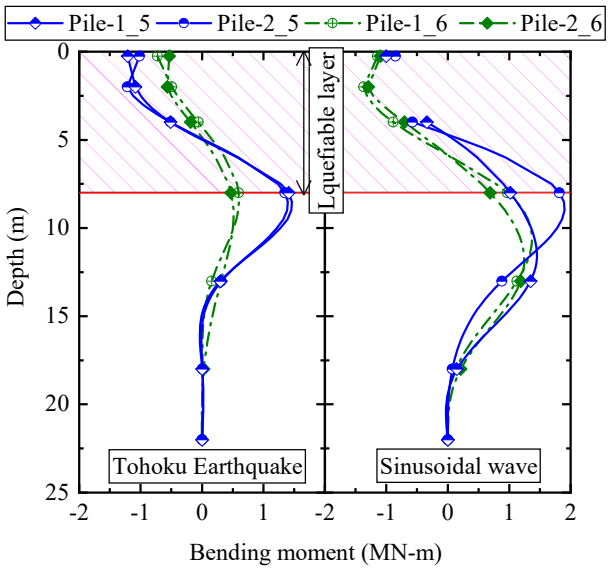

778

779 Fig. 20: Bending moment profiles for Pile-1 and Pile-2 in C-5 and C-6 when the piles experience

780 the maximum bending moment.

781

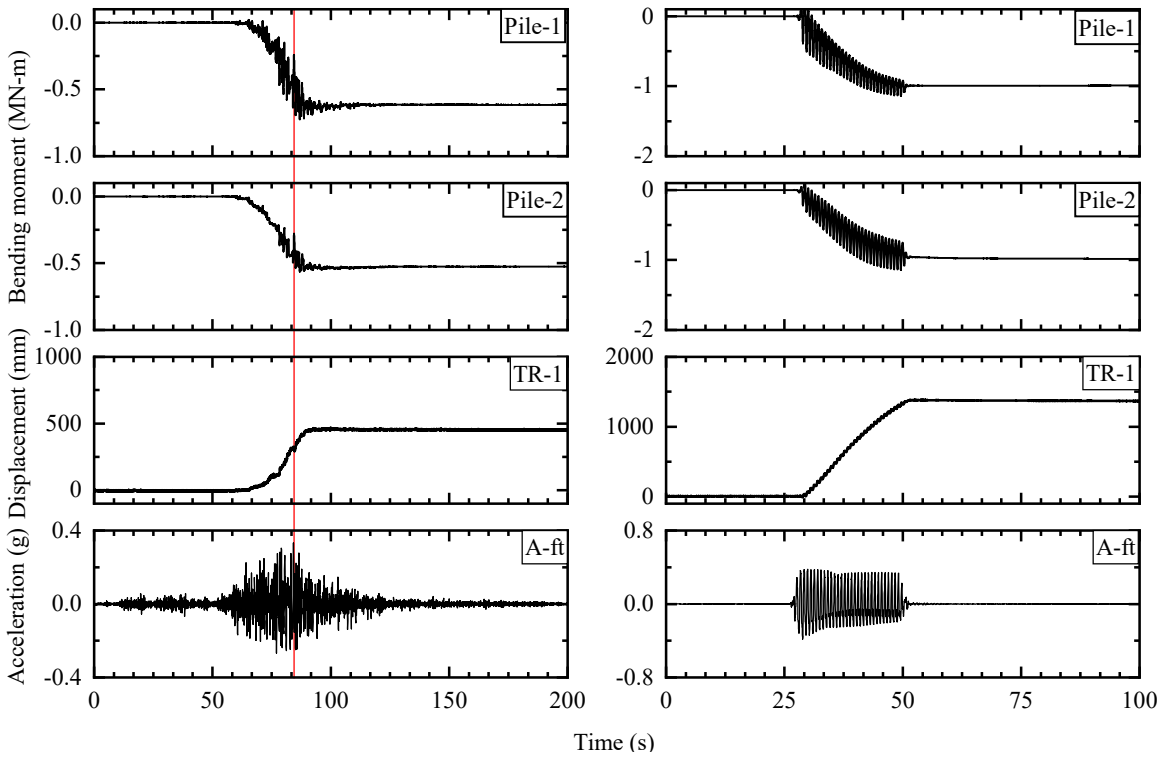

782

783 Fig. 21: Time histories of bending moment near the head of the Pile-1 and Pile-2 (at a depth
784 of 0.25 m), horizontal displacement at TR-1 (2.0 m below the crest of the abutment) and
785 acceleration of the abutment footing (A-ft) in C-6.

786

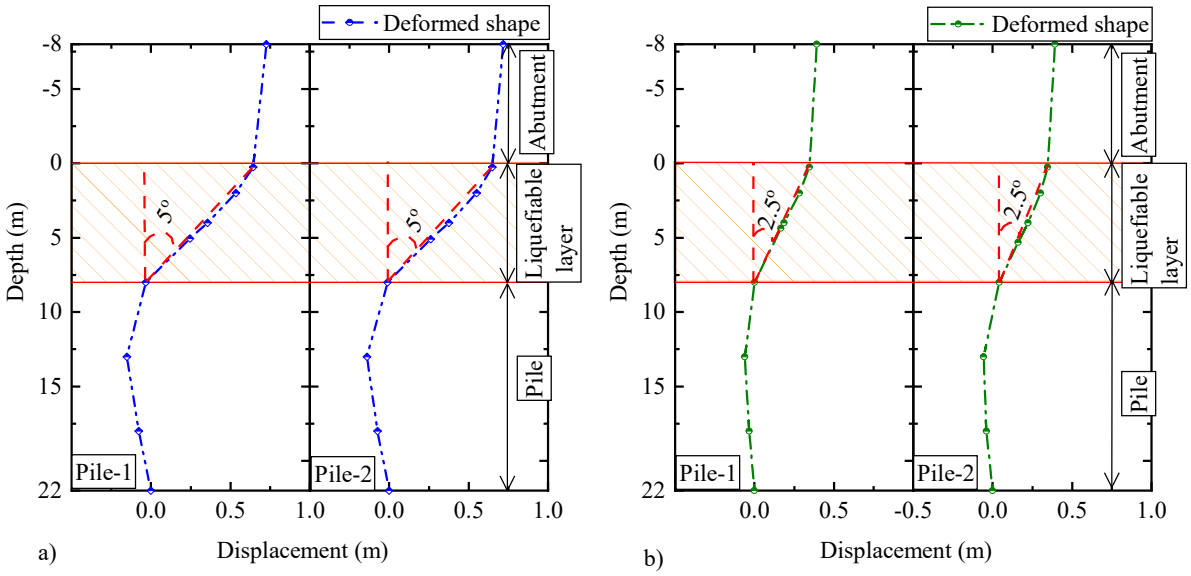

787

788 Fig. 22: Displacement profiles of Pile-1 and Pile-2 along with the abutment in a) C-5 (without

789 sheet pile) and b) C-6 (with sheet pile) when the piles experience the maximum bending

790 moment during Tohoku Earthquake.

791